Dual topologies of myotomal collagen XV and Tenascin C act in concert to guide and shape developing motor axons

Laurie Nemoz-Billet, Martial Balland, Laurent Gilquin, Benjamin Gillet, Isabelle Stévant, Emilie Guillon, Sandrine Hughes, Gilles Carpentier, Elisabeth Vaganay, Frédéric Sohm, et al.

PNAS RESEARCH ARTICLE | DEVELOPMENTAL BIOLOGY

Dual topologies of myotomal collagen XV and Tenascin C act in concert to guide and shape developing motor axons

Laurie Nemoz-Billet[a], Martial Balland[b], Laurent Gilquin[a], Benjamin Gillet[a], Isabelle Stévant[a], Emilie Guillon[a], Sandrine Hughes[a], Gilles Carpentier[c], Elisabeth Vaganay[a], Frédéric Sohm[a], Vladimir Misiak[b], Mary-Julieth Gonzalez-Melo[a], Manuel Koch[d], Yad Ghavi-Helm[a], Sandrine Bretaud[a,1], and Florence Ruggiero[a,1]

Edited by Alexander Schier, Universitat Basel, Basel, Switzerland; received August 23, 2023; accepted February 26, 2024

During development, motor axons are guided toward muscle target by various extrinsic cues including extracellular matrix (ECM) proteins whose identities and cellular source remain poorly characterized. Here, using single-cell RNAseq of sorted GFP$^+$ cells from *smyhc1:gfp*-injected zebrafish embryos, we unravel the slow muscle progenitors (SMP) pseudotemporal trajectory at the single-cell level and show that differentiating SMPs are a major source of ECM proteins. The SMP core-matrisome was characterized and computationally predicted to form a basement membrane–like structure tailored for motor axon guidance, including basement membrane–associated ECM proteins, as collagen XV-B, one of the earliest core-matrisome gene transcribed in differentiating SMPs and the glycoprotein Tenascin C. To investigate how contact-mediated guidance cues are organized along the motor path to exert their function in vivo, we used microscopy-based methods to analyze and quantify motor axon navigation in *tnc* and *col15a1b* knock-out fish. We show that motor axon shape and growth rely on the timely expression of the attractive cue Collagen XV-B that locally provides axons with a permissive soft microenvironment and separately organizes the repulsive cue Tenascin C into a unique functional dual topology. Importantly, bioprinted micropatterns that mimic this in vivo ECM topology were sufficient to drive directional motor axon growth. Our study offers evidence that not only the composition of ECM cues but their topology critically influences motor axon navigation in vertebrates with potential applications in regenerative medicine for peripheral nerve injury as regenerating nerves follow their original path.

extracellular matrix | motor axon pathfinding | zebrafish | muscle progenitors | scRNA seq

Significance

En route to their muscle targets, growing motor axons are guided by a combination of diffusible and contact-mediated cues that attract or repel axons. Notably, motor axon navigation is locally influenced by extracellular matrix signposts that pave their trajectories. The repertoire and function of these contact-mediated cues and their cellular source are still under investigation. Using zebrafish, we show that differentiating muscle progenitors represent an important source of extracellular matrix cues. Our study reveals that the attractive Collagen XV-B is organized in a permissive route delimited by the repulsive Tenascin C to allow accurate navigation of motor axons. Our findings provide insights into how extracellular matrix participates in axonogenesis with interest in nerve regenerative medicine for peripheral nerve injury.

During development, axons of motor neurons follow stereotypical trajectories to their muscle targets, guided by various molecular cues. The extracellular matrix (ECM) can influence motor axon navigation by providing external chemical and mechanical guidance cues to developing axons, attracting or repelling them. Among them are the well-known diffusible chemical cues, netrins, and semaphorins, that likely collaborate with other extracellular cues to guide developing axons (1). Yet, contact guidance cues, which are immobilized ECM proteins, remain poorly documented. The zebrafish has proven to be a powerful animal model to investigate peripheral nervous system development and more specifically motor axon navigation (2). There are three types of primary motor neurons per spinal cord hemisegment that are identified by their cell body position in the spinal cord: the rostral primary (RoP), the middle primary (MiP), and the caudal primary (CaP). At 17 hours post- fertilization (hpf), primary motor axons initiate outgrowth and exit the spinal cord, a process that is pioneered by the CaP. Next, they project through a common path and pause at the choice point which corresponds to an intermediate target located at the level of the horizontal myosepta. Then, the RoP, MiP, and CaP axons diverge to innervate specific territories, respectively the lateral, dorsal, and ventral myotomes. The myotome is an important source of guidance cues for developing motor axons (2). In particular, because of their position in the trajectory of the future growing axons, the slow muscle precursors (SMPs) (a.k.a adaxial cells) and muscle pioneers (MPs) have been shown to play a pivotal role in motor axon navigation (3, 4). As the myotome develops and before motor axon extension, SMPs stack, elongate, and traverse the myotome to reach its periphery where they eventually differentiate into slow superficial fibers (5). Only a subset of SMPs differentiate into MPs and remain located adjacent to the notochord (6). As motor axons exit from the spinal cord, they extend through an ECM path mainly produced and deposited locally by SMPs, supposed to be the major source of ECM guidance cues (2).

The ECM forms complex and intricate protein networks whose composition and spatial organization are closely related to their function in tissues (7). Chondroitin sulfate

Author contributions: L.N.-B., M.B., L.G., I.S., G.C., S.B., and F.R. designed research; L.N.-B., M.B., L.G., B.G., E.G., S.H., G.C., E.V., F.S., V.M., M.-J.G.-M., and S.B. performed research; M.K. and Y.G.-H. contributed new reagents/analytic tools; L.N.-B., M.B., L.G., G.C., F.S., S.B., and F.R. analyzed data; I.S. provide conceptual advice; S.H., G.C., and Y.G.-H. proofread the manuscript; F.R. secure funding; and L.N.-B., L.G., S.B., and F.R. wrote the paper.

The authors declare no competing interest.

This article is a PNAS Direct Submission.

[1]To whom correspondence may be addressed. Email: sandrine.bretaud@ens-lyon.fr or florence.ruggiero@ens-lyon.fr.

This article contains supporting information online at https://www.pnas.org/lookup/suppl/doi:10.1073/pnas.2314588121/-/DCSupplemental.

Published March 19, 2024.

proteoglycans and Tenascin-C (TnC) are both expressed by SMP and have been identified as important guidance cues for zebrafish motor axons (8–10). Notably, TnC morphants display abnormal extrabranching axons indicating a role of TnC as a repulsive local molecular cue that guides motor axons (10). Collagens also play a role in axon navigation in the zebrafish central nervous system, as well as in the peripheral nervous system (11). Defects in motor axon navigation were observed both in Collagen XVIII morphants (12) and Collagen XIX mutants (*stumpy* mutants) (13). More recently, we identified Collagen XV-B (ColXV-B) as an attractive contact guidance cue that is deposited in the motor path by the SMPs before they migrate at the myotome periphery (14). In invertebrates, the absence of the ColXV/ColXVIII orthologs, Dmp/Mp in drosophila and cle-1 in *Caenorhabditis elegans*, also led to defects in motor axon navigation (15, 16), suggesting that the role of ColXV in axonogenesis is well conserved across species. All three collagens, the multiplexins ColXV and ColXVIII, and the FACIT (Fibrillar-associated Collagen with Interrupted Triple helix) ColXIX, are basement membrane zone (BMZ)-associated collagens (7) suggesting that the motor axon trajectory is lined with a BMZ-like structure.

Although a few ECM molecules have been described as contact guidance cues, the full composition and specifically their organization in the ECM motor path remain unresolved. To fill this gap, we first performed a single-cell RNA sequencing (scRNAseq) analysis of differentiating SMPs to characterize the matrisome of SMPs. Bioinformatics analysis of the data shows that differentiated SMPs both express BM-toolkit genes and specific core-matrisome genes involved in motor axon navigation that together can organize into a BMZ-like structure tailored for motor axon guidance. In support of this, image analysis of immunofluorescence staining combined with loss of function experiments and biomechanics and bioengineering analysis revealed that ColXV-B, the earliest core-matrisome gene product expressed by differentiated SMPs, creates a favorable microenvironment for axon growth and navigation by influencing ECM motor path stiffness and topology. Our study put forward a paracrine role for SMP in shaping ECM path critical for future motor axon navigation toward their muscle target.

Results

Single-Cell Profiling Unravels the Dynamics of SMP Differentiation. Before their final differentiation into slow superficial fibers, SMPs undergo a series of morphological changes, from pseudoepithelial organization to elongated premigratory architectures, as the myotome matures (Fig. 1*A*). While the SMP stereotypical behaviors are well characterized, their related-gene signatures remain unknown. We thus first aimed at characterizing the trajectory and gene signatures of SMP differentiation using scRNAseq. We took advantage of the rostro-caudal polarity of the segmented somites and the segmentation clock during which one additional somite is formed every 30 min to isolate SMPs at different stages of their differentiation in the same embryo at 18 hpf. To enrich SMP cell population in 18 hpf trunk homogenates, we injected one-cell stage embryos with *smyhc1:gfp* construct containing the green fluorescent protein open reading frame under the control of the slow muscle marker *smyhc1* (*slow myosin heavy chain 1*) promoter and the cell suspension obtained from injected embryos was used to sort GFP-positive cells (*smyhc1* expressing cells) and perform scRNAseq (Fig. 1*B*). Unbiased clustering analysis of our scRNAseq data revealed 18 clusters. Four clusters were enriched for cells that expressed *smyhc1* and *prdm1a*, two specific markers of the slow muscle lineage: cluster 1 (491 cells), cluster 5 (347 cells), cluster 10 (175 cells) and cluster 11 (172 cells) (Fig. 1*C*). The mapping against the zebrafish genome containing the *gfp* gene indicated that *smyhc1* expressing cells exhibit a high expression of *gfp* confirming the SMP identity of *smyhc1* positive cells (*SI Appendix*, Fig. S1*A*). We thus further focused on the analysis of these four clusters annotated as slow muscle lineage derived-cells.

We next decided to construct the pseudotemporal SMP differentiation trajectory based on the expression of myogenic regulatory factors that are known to be differentially expressed during SMP differentiation. The increasing level of *smyhc1* in each of the four clusters confirmed their level of maturation (Fig. 1*D*). Previous in situ analyses showed that the expression of *prdm1a* in tail-bud stage and 18 hpf embryos begins at the interleafing/pseudoepithelial SMP stages. It then reaches a peak of expression in apical constriction/broad SMP stages and decreases in premigrating myoblasts of anterior somites (17). Together, these temporal and spatial myogenic gene expression data suggest that the less mature myoblasts present in cluster 10 very likely correspond to interleafing/pseudoepithelial SMP stages while the premigrating cells are present in cluster 1. We conclude that the peak of *prdm1a* expression observed in cluster 11 cells corresponds to the apical constriction/broad SMP stages and that the decrease in *prdm1a* expression observed in cluster 5 intermediate SMPs corresponds to the elongated premigratory stage (Fig. 1*D*). As a confirmation of the robustness of the method used to allocate SMPs trajectory to the different clusters, our scRNAseq data clearly subclustered a population of 70 cells in the premigrating cluster that are identified as muscle pioneers (MP) cells as they additionally and specifically expressed the MP *engrailed1a* (*en1a*) marker (Fig. 1*E*). Furthermore, the in situ hybridization data obtained by Thisse and coworkers (18–20) confirm the transcriptional dynamics of some of the cluster-specific SMP genes identified in our study (top 20 differentially expressed genes) (*SI Appendix*, Fig. S1*B*), and thus validate our scRNAseq data.

In conclusion, cluster 10 corresponds to the less-differentiated myoblasts and cluster 1 to the most differentiated ones, while clusters 11 and 5 respectively comprise cells of successive intermediate stages of differentiation. By resolving SMPs pseudotemporal trajectory at the single-cell level, specific gene expression signatures could be ascribed to the differentiating SMP morphological architectures.

Differentiating SMP Express BM-Like Specialized ECM Genes. We further aimed at characterizing the ECM gene expression landscape of differentiating SMPs. Using our in silico zebrafish matrisome database (21), we determined that SMPs globally express 9% of total zebrafish matrisome genes (91/1,004). Among these ECM genes, SMPs expressed both core matrisome genes (36/335) and matrisome-associated genes (55/669) which comprise ECM-affiliated genes, ECM regulators and secreted factors (Fig. 2*A* and *SI Appendix*, Tables S1–S4). The less-differentiated SMPs (cluster 10) mainly express matrisome-associated genes (34 genes among 51 matrisome genes), especially ECM regulators and secreted factors (13 and 17, respectively). Notably, expression of ECM regulators such as *mmp2* and *mmp14a* in cluster 10 cells indicate an ECM remodeling of the cell microenvironment. On the contrary, elongated premigratory SMPs (cluster 5) predominantly express core matrisome genes (29 genes among 56 matrisome genes), suggesting that these SMPs are the main cell source of ECM cues (Fig. 2*A*). Based on the GO term "axon guidance" (GO:0007411) and data from the literature, we found that SMPs, independently of their differentiating stages, express core matrisome genes and matrisome-associated genes that are known to be involved in axon guidance such as *agrn*, *col15a1b*, *col18a1a*, *col19a1*, *lama5*, *ntn1a*, and *tnc* as well as the

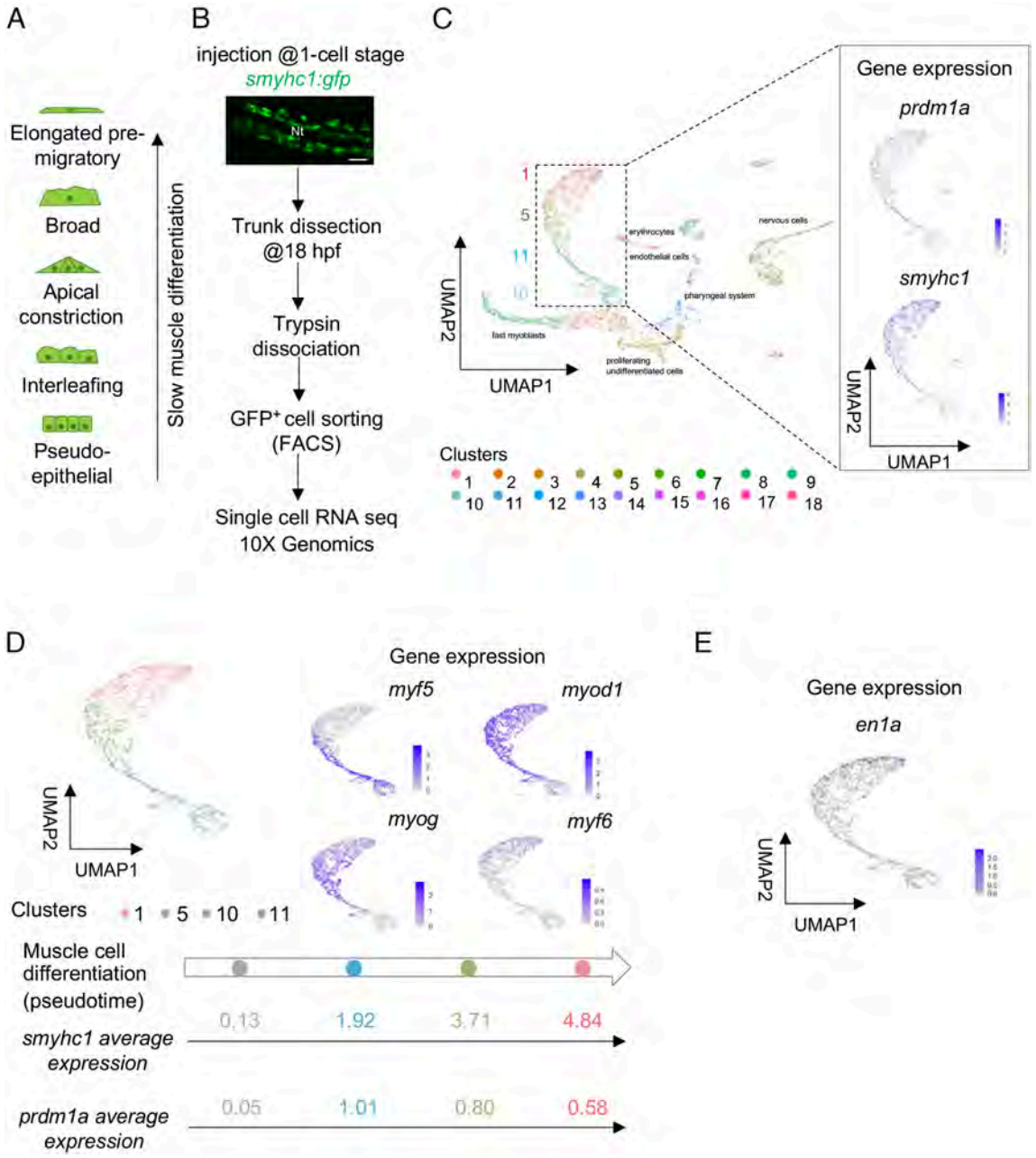

Fig. 1. Differentiating SMPs display specific gene expression signatures. (*A*) Schematics of the morphological series of differentiating SMPs in 18 hpf embryos. (*B*) Schematic representation of the protocol used for scRNAseq; Confocal projection of *smyhc1:gfp* expression in a living 18 hpf embryo. Dorsal view. (Scale bar, 50 μm.) Nt, notochord. Anterior is left. (*C*) UMAP plot obtained after mapping on the zebrafish genome and clusterization of isolated GFP$^+$ cells (*Left* panel); UMAP feature plots showing expression patterns of slow muscle lineage markers *prdm1a* and *smyhc1* (*Right* panel). (*D*) UMAP plot obtained after isolation of the clusters corresponding to SMP lineage; UMAP feature plots showing the expression pattern of myogenic regulatory factors in differentiating SMPs (*Right* panel); pseudotime trajectory of differentiating SMPs; *smyhc1* and *prdm1a* average expression in each cluster (*Bottom* panel). Colors represent different clusters. (*E*) UMAP feature plot showing the expression of the MP marker *en1a*.

classic guidance cues *cxcl12a*, *cxcl12b*, *plxna3*, *plxnb1a*, *sema4ba,* and *vegfaa* (*SI Appendix*, Tables S1–S4).

Finally, we characterized the matrisome of the MP cells that are described as intermediate targets for growing axons (3). MP predominantly express core matrisome genes akin to the more mature SMPs (clusters 1 and 5) differing from SMPs core matrisome genes by only 4 additional genes: *col1a2, colq, lgi1a, and vwa2* (*SI Appendix*, Table S5). STRING-based protein interactions were used to build the interactome of the total core matrisome genes expressed by SMPs. This interaction network reveals a major hub (in red) composed of 20 genes including those encoding the toolkit BM proteins collagen IV, laminins, and nidogens, suggesting that the motor axon path ECM mainly consists in a specialized BM. Interestingly, STRING analysis and clustering also unravel a protein interactions network between the main hub and BM-associated proteins all previously described as ECM guidance cues, TnC, ColXVIII, ColXIX, and ColXV-B (10, 12–14) (Fig. 2*B*). Our data show that prior migrating to their final destination at the myotome periphery, SMPs display strict temporal expression of gene encoding BM and BM-associated axon guidance local cues. These ECM proteins likely then assemble into a unique BM-like structure and organization that is required for its specialized downstream function.

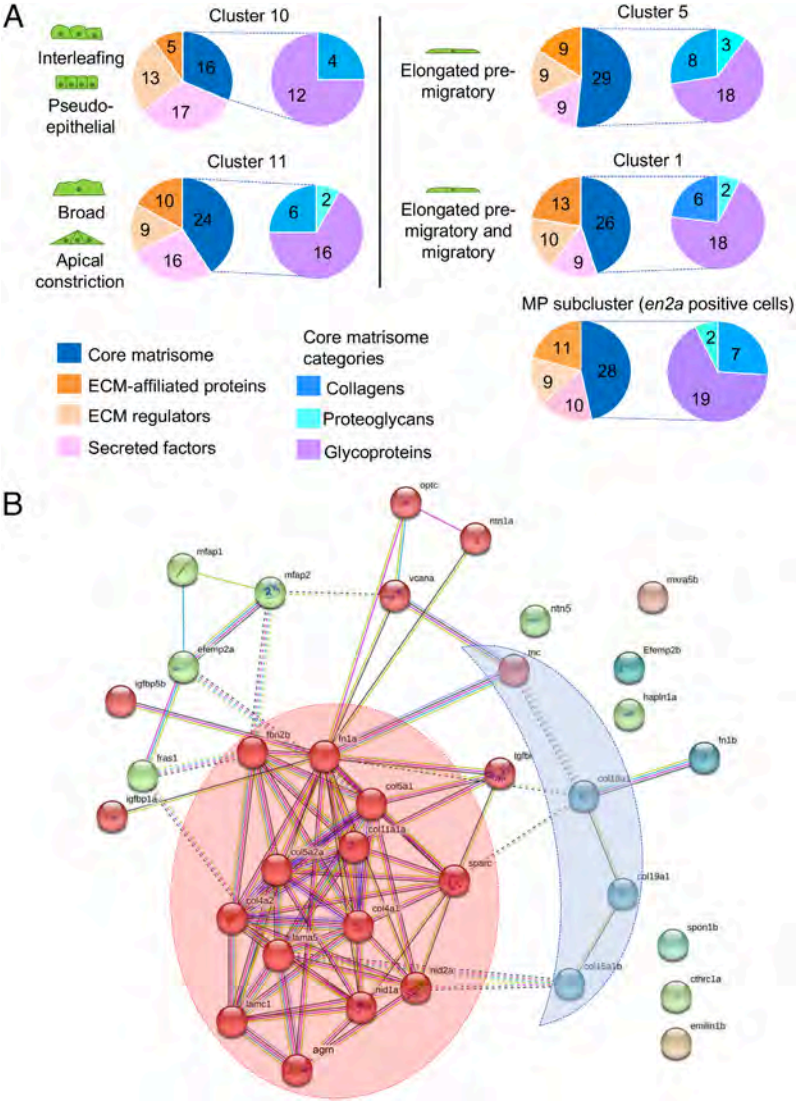

Fig. 2. Characterization of differentiating SMP matrisomes. (*A*) *Left* pie charts represent the number of matrisome genes expressed in each cluster and classified by categories, *Right* pie charts represent the number of core-matrisome genes expressed in each cluster and by subcategories. (*B*) Protein–protein interaction network analysis of the total core matrisome genes expressed by SMPs with STRING database. The protein interaction network of the 36 core-matrisome genes was created with an enrichment *P*-value $<10^{-16}$. Clusters were generated using a MCL inflation parameter of 2. One color represents one cluster. Two hubs of interest are highlighted: BM-toolkit (red) and BM-associated genes (blue).

The TnC and ColXV-B Guidance Cues Exhibit Dual Topology that Confines the Motor Axon Trajectory. To test this hypothesis, we decided to visualize the spatial organization of the BM-associated proteins with confocal microscopy. *tnc*, *col18a1a,* and *col15a1b* all start to be expressed in apical constriction/broad SMPs (cluster 11; *SI Appendix*, Table S2), while the onset of *col19a1* expression occurs in elongated premigratory SMPs (cluster 5; *SI Appendix*, Table S3). As TnC and ColXV-B exhibit functional duality (10, 14) as they display opposite function within this peculiar biological context, we reasoned that these two immobilized guidance cues organize in well-defined topologies to appropriately guide motor axons. We thus performed double immunostaining of 27 hpf *mnx1:gfp* embryos to directly visualize trunk motor axons with antibodies targeting ColXV-B (*SI Appendix*, Fig. S2) and Tenascin C. Our double immunostaining unveils that TnC and ColXV-B display distinctive and mutually exclusive spatial expression patterns. While ColXV-B is deposited along the motor axon path in a ladder fashion (Fig. 3*A*) as we previously showed (14), TnC is restricted to the choice point where it forms a channel that delineates the motor axon path (Fig. 3*A*). Orthogonal views confirm the dual topology of the ColXV-B/TnC deposits (Fig. 3*A*). Whereas ColXV-B intermittently wraps motor axon all along its trajectory, TnC forms borders which vertically delimit the motor axon path (Fig. 3*A*). We thus conclude that SMPs produce the duo of repulsive and attractive ECM guidance cues, TnC and ColXV-B respectively, that are spatially organized into distinct topologies to control locally motor axon trajectory.

To verify whether this topology is decisive for motor axon shaping and navigation, we reproduced the dual topology of TnC and ColXV-B using the Alveole lab technology (22). This technology relies on photopatterning proteins to create reproducible tailored in vitro environments that mimic native cell microenvironments. To do so, we used recombinant ColXV-B and TnC proteins produced in HEK293 cells (mrTnC) (*SI Appendix*, Fig. S2*A*). The proper organization of the resulting double bioprinted ECM micropatterns was assessed by immunostaining and exhibited the expected topology: ColXV-B in the central route delineated by TnC deposits (Fig. 3*B*). Micropatterns in which TnC borders were replaced with ColXV-B were also designed to be used as controls. We next seeded isolated GFP^+ motor neurons from 24 hpf *mnx-1:gfp* embryos onto the micropatterns for 24 h to allow neurites to grow (Fig. 3*C*). The growth of GFP^+-neurites was then quantified as the total number of pixels in ColXV-B and TnC areas (Fig. 3*D*). The results show that neurites extend significantly more in the ColXV-B central route than in the TnC borders, whereas no difference was observed when motor neurons were seeded onto ColXV-B control micropatterns (Fig. 3*D*). Interestingly, the repulsive role of TnC seems to be evolutionary conserved as we used

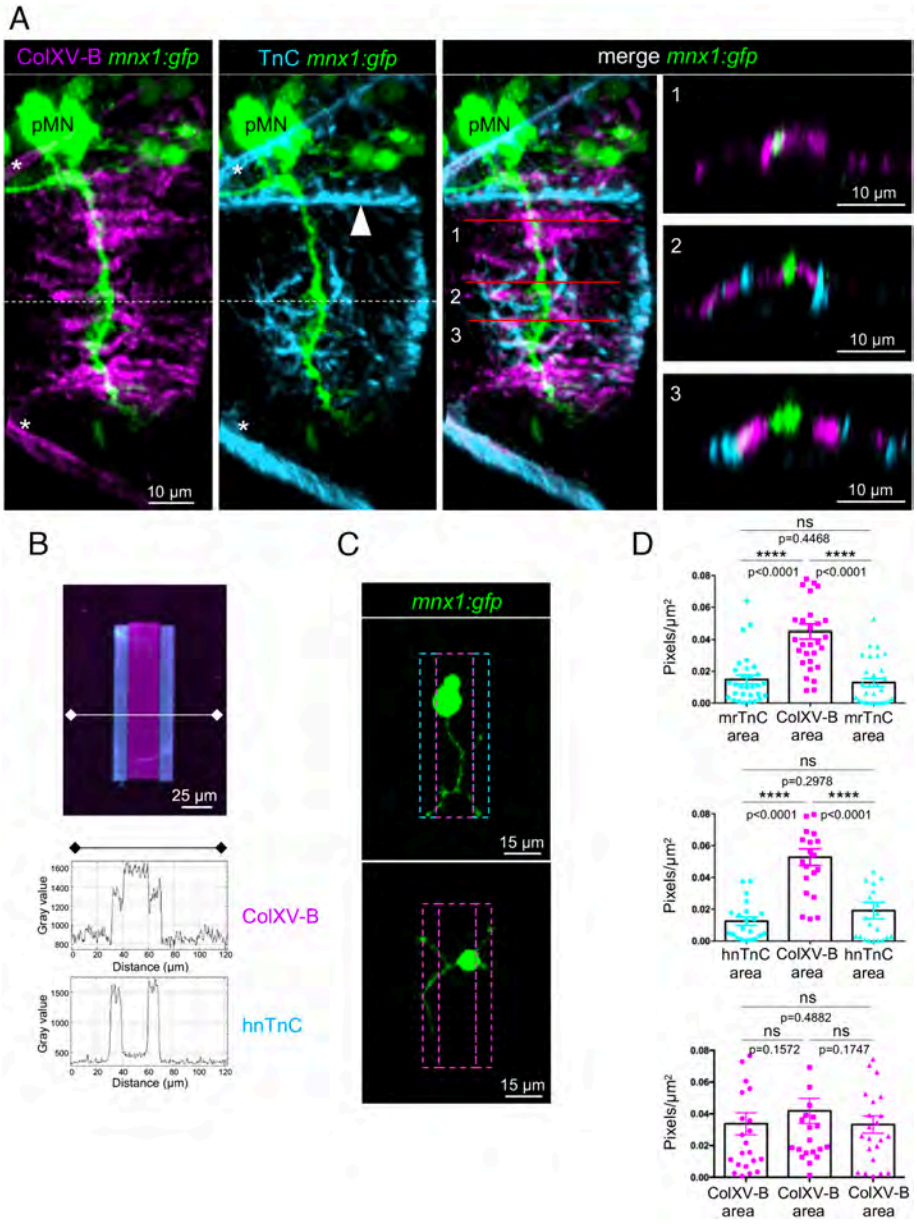

Fig. 3. The motor axon trajectory is formed by a central ColXV-B path delimited by TnC borders. (*A*) 3D Imaris images of whole-mount immunostaining of 27 hpf *mnx1:gfp* embryos with anti-rNC1 (magenta, ColXV-B), anti-TnC (cyan), and anti-GFP antibodies (green, motor neurons). *Left* panel, lateral views; *Right* panel, orthogonal views; anterior is left. The dotted line shows the horizontal myosepta. Asterisks indicate the vertical myosepta. The arrowhead points to the dorsal edge of the notochord. Numbers indicate the level of virtual orthogonal sections (*B*) Double immunostaining of 45 × 70 µm ColXV-B/TnC micropatterns with anti-rNC1 (magenta, ColXV-B) and anti-TnC (cyan), plot profile of ColXV-B and TnC staining (Fiji software). Micropattern with human native TnC (hnTnC) is shown. (*C*) Live confocal images of motor neurons 24 h after seeding on 31 × 70 µm ColXV-B/TnC micropatterns (*Top* panel) and ColXV-B control micropatterns (*Bottom* panel). (*D*) Quantification of the number of pixels corresponding to the neurites for each ColXV-B or TnC area expressed in percentage of the total micropattern area. *Top* panel, double ColXV-B/murine recombinant TnC (mrTnC) micropatterns; n = 30; *Middle* panel, ColXV-B/ hnTnC double micropatterns, n = 21; *Bottom* panel, ColXV-B control micropatterns, n = 23. Statistical analysis was performed using one-way ANOVA and Tukey's multiple comparisons tests. ****$P < 0.0001$; ns, not significant. Error bars are mean ± SEM.

murine or human TnC for the preparation of the micropatterns (Fig. 3*D*). Our finding unambiguously demonstrates the importance of well-defined ECM architectural cues in the vicinity of growing axons to locally instruct axon growth.

ColXV-B Is Required for Modeling TnC-Specific Architecture in the Motor Path. ColXV-B was reported to act as an ECM organizer (23). We thus assumed that ColXV-B could be necessary for modeling ECM of the motor path. To test this assumption, we first examined in detail the temporal expression pattern of *tnc*, *col18a1a,* and *col15a1b* in the less-differentiated cells of cluster 11 identified based on the *smyhc1* expression level (*SI Appendix*, Fig. S3*A*). We identified *col15a1b* as the earliest gene expressed by differentiating SMPs within cluster 11, followed by *col18a1a* and then *tnc* (*SI Appendix*, Fig. S3*A*), while *col19a1* starts to be expressed in more mature SMPs in cluster 5 (*SI Appendix*, Table S3). Only the expression of *col15a1b* and *tnc* persists in the most differentiated SMPs in cluster 1 (*SI Appendix*, Table S4). The subclusterization of clusters 5 (elongated premigratory SMPs) and 11 (apical constriction/ broad SMPs) results in the emergence of five subclusters (1a-5a) (*SI Appendix*, Fig. S3*B*). Examining *col15a1b* and *tnc* expression levels in each cell within a given cluster indicates their coexpression in almost all cells in subclusters 1a, 2a, and 4a, while cells in subclusters 3a exhibit prominent *col15a1b* expression (*SI Appendix*,

Fig. S3*D*). In all subclusters, only a few cells expressed *tnc* alone. Combining these data with *smyhc1* gene expression in each subcluster (*SI Appendix*, Fig. S3*C*), we confirmed that *col15a1b* is expressed before *tnc* expression at early stage of SMP differentiation and that the most differentiated cells predominantly coexpressed both genes. To spatially identify these subpopulations, we conducted smi-FISH experiments using *col15a1b* and *tnc* probes in 18 hpf *smyhc1:gfp* embryos, enabling visualization of all SMP differentiation stages within the same embryo. As expected, *col15a1b* was detected caudally in early stages, while the *tnc* signal emerged predominantly in the middle and posterior part of the trunk, in apical-broad cells, along with an increase in *col15a1b* transcripts (*SI Appendix*, Fig. S3*E*).

In order to determine whether ColXV-B is necessary for organizing motor path ECM, the architecture of TnC deposits was analyzed in 27 hpf *col15a1b*$^{-/-}$ mutant embryos. Lack of ColXV-B results in the apparent loss of the TnC characteristic organization in the motor path and TnC immunoreactivity abnormally spread over the ColXV-B free-area (Fig. 4*A*). This is accompanied by a significant intersubject variability in TnC fluorescence intensity (*SI Appendix*, Fig. S4*A*). To verify whether the channel-like organization of TnC in the motor path is lost in the absence of ColXV-B, an unsupervised clustering analysis was conducted on 120 images to group images with a similar distribution of TnC along the motor path. The distribution profile features a characteristic bimodal distribution shape when TnC exhibits a typical channel-like organization as in most images of the wild type compared to *col15a1b*$^{-/-}$ embryos (Fig. 4*B*). All analyses were blind to embryo types to avoid bias. Clustering analysis reveals two major clusters, clusters 1 and 2 and two minor clusters 3 and 4 (Fig. 4*C*, histogram). The interactive visualization of the cluster partition is available at https://igfl.gitbiopages.ens-lyon.fr/ruggiero/zebrafishtnc/. Cluster 2 (mauve) contains 88% images of *col15a1b*$^{-/-}$ mutant embryos that were shown a posteriori to exhibit no specific distribution whereas cluster 1 (green) consists in 73% images of wt embryos with a bimodal shape of TnC distribution (Fig. 4*C*). Accordingly, axons length was significantly reduced in cluster 2 compared to cluster 1 (*SI Appendix*, Fig. S4*B*). Cluster 4 (red) comprises few images among them some display a curved channel shape. Cluster 3 (yellow) is equally composed of images of wt and mutant embryos for which TnC deposits display no specific distribution.

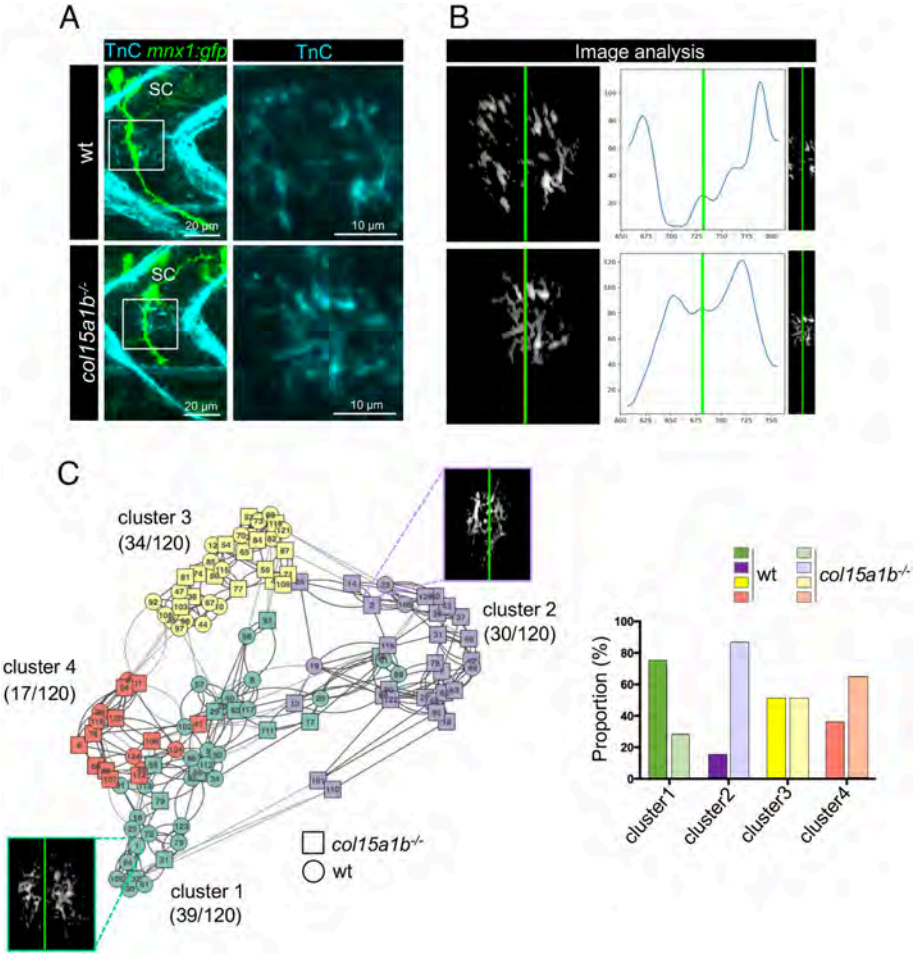

Fig. 4. Lack of ColXV-B compromises TnC channel-like organization in the motor axon path. (*A*) *Left* panel, whole-mount immunostaining of 27 hpf *mnx1:gfp* and *col15a1b*$^{-/-}$*;mnx1:gfp* embryos with anti-TnC (cyan) and anti-GFP (green, motor axons) antibodies. *Right* panel, zoom of boxed images (*Left*) showing detail of Tnc staining. (*B*) Three-plot representation of one wild type and *col15a1b*$^{-/-}$embryo. *Left* panel, 8-bit image resulting from the TnC deposition assessment. *Right* panel, 8-bit image resulting from the truncation step for TnC channel organization analysis. Curves show TnC distribution along the motor path (blue curve) estimated by vertically summing nonzero pixels then smoothed by a Gaussian filter. In all images, the green line marks the center of the TnC channel. n^{wt} = 11 embryos, $n^{col15a1b-/-}$ = 13 embryos, for each embryo 5 axons are analyzed. (*C*) *Left* panel, Clustering analysis of 120 images of TnC staining in wt (circle) and *col15a1b*$^{-/-}$ (square) mutants. One color represents one cluster and numbers in brackets indicate the total number of images for each cluster out of the 120 images analyzed. Representative eight-bit image is shown for cluster 1 (green) and cluster 2 (mauve). *Right* panel, Histogram showing the proportion of wt and *col15a1b*$^{-/-}$ mutant embryos in each cluster; For a same color, dark color represents wt embryos and light color represents *col15a1b*$^{-/-}$ embryos.

Together with its earliest expression in differentiating SMPs (*SI Appendix*, Fig. S3), these results show that initial expression and deposition of ColXV-B is required for correct TnC organization in the motor path. We thus assumed that absence of TnC expression will not affect ColXV-B organization. To test this, we generated and characterized a *tnc* knock-out line using CrispR/Cas9 method and verified with immunofluorescence its complete absence in $tnc^{-/-}$ embryos (*SI Appendix*, Fig. S5 *A* and *B*). No statistically significant difference in ColXV-B deposition was observed in the absence of TnC (*SI Appendix*, Fig. S5*C*). ColXV-B plays a critical role in confining the TnC deposition to the motor path borders that is essential for locally guide growing motor axons.

ColXV-B and TnC Coordinate to Regulate Axon Growth and Branching. As the lack of ColXV-B results in TnC disorganization in the motor path, we then asked whether the $col15a1b^{-/-}$ phenotype that we previously reported (14) is an indirect consequence of the loss of the characteristic TnC topology in the motor path. We reasoned that if it is the case, the motor axon phenotype of the $tnc^{-/-}$ embryos should be identical to the $col15a1b^{-/-}$ phenotype. We thus examined the motor axon phenotype of our newly generated $tnc^{-/-}$ line (no TnC, *SI Appendix*, Fig. S5*B*) and compared the potential defects in axon navigation to the ones observed in the $col15a1b^{-/-}$ mutants (loss of TnC architecture) (Fig. 5*A*). While the reduction of axon length appeared to be associated only to the lack in *col15a1b* expression (Fig. 5*B*), measurements of the total length of axon branches and branching points after normalization to axon length signify that both $tnc^{-/-}$ and $col15a1b^{-/-}$ embryos abnormally develop excessive axon branches at 27 hpf, even though the phenotype was statistically aggravated in $col15a1b^{-/-}$ embryos (Fig. 5 *D*–*F*). No change in the distance between axons was observed in mutants indicating that axons were not misrouted in absence of TnC or ColXV-B (Fig. 5*C*). Together, these data suggest that ColXV-B influences axonal navigation through both TnC-dependent and TnC-independent mechanisms.

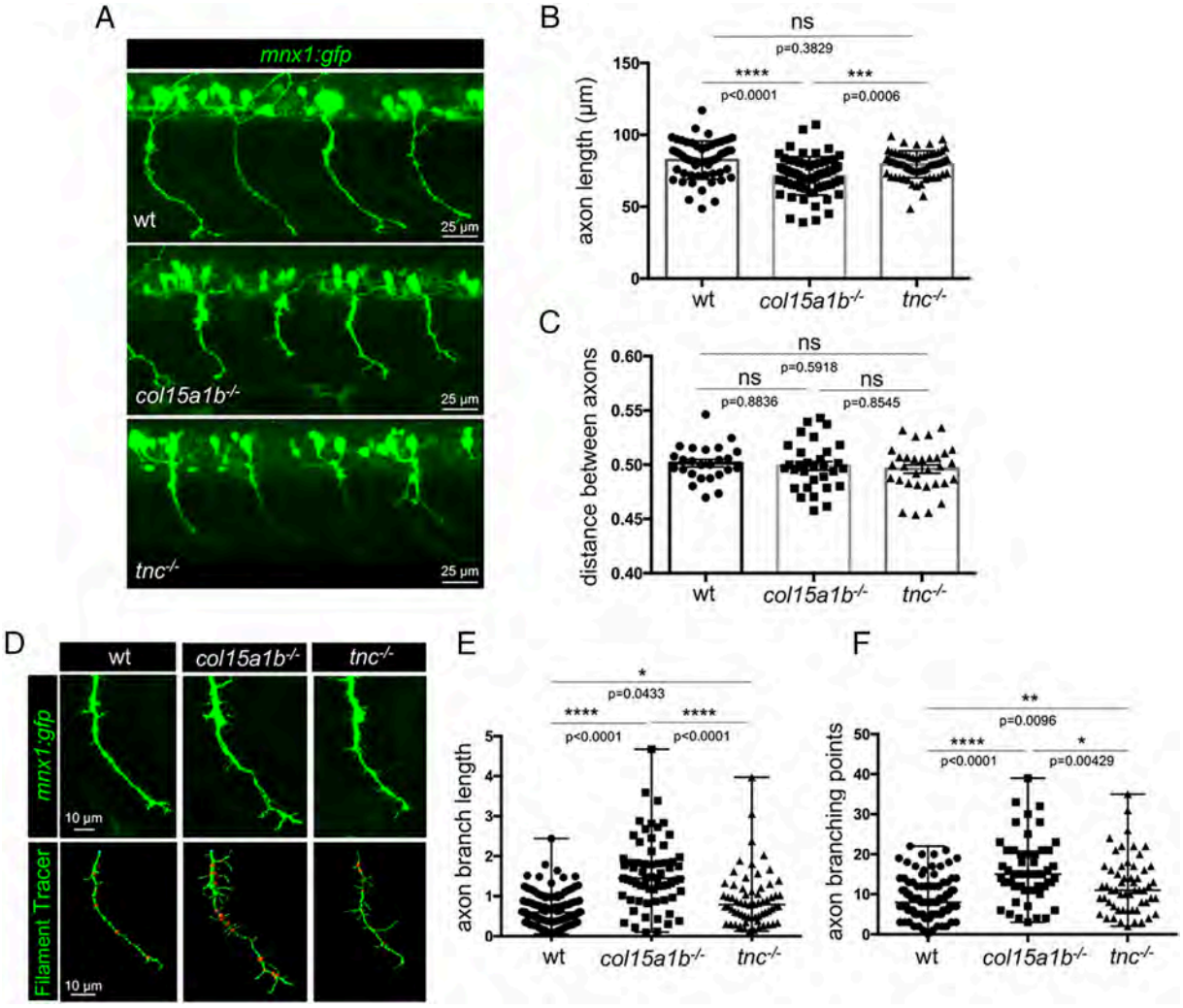

Fig. 5. $col15a1b^{-/-}$ and $tnc^{-/-}$ embryos both display abnormal extrabranching phenotype. (*A*) whole-mount immunofluorescence of 27 hpf wild-type, $col15a1b^{-/-}$, and $tnc^{-/-}$ mutant embryos with gfp antibodies (motor neurons, green). (*B*) Quantification of the axon length, n^{wt} = 11 embryos, 55 axons, $n^{col15a1b-/-}$ = 13 embryos, 65 axons, $n^{tnc-/-}$ = 13 embryos, 64 axons; (*C*) Distance between axons normalized to the distance between the two adjacent somites (in µm), n^{wt} = 9 embryos, 25 somites, $n^{col15a1b-/-}$ = 10 embryos, 31 somites, $n^{tnc-/-}$ = 10 embryos, 31 somites. Statistical analyses in *B* and *C* were performed using Tukey's multiple comparisons test. Mean and SD are presented. (*D*) Whole-mount immunostaining of 27 hpf wt, $tnc^{-/-}$ and $col15a1b^{-/-}$ mutant embryos with anti-GFP to visualize individual motor axons (green) and their corresponding 3D representation using filament tracer (Imaris software). (*E*) Quantification of branching length normalized to axon length, n^{wt} = 24 embryos, 118 axons, $n^{col15a1b-/-}$ = 13 embryos, 64 axons, $n^{tnc-/-}$ = 13 embryos, 64 axons (*F*) branching point normalized to axon length, n^{wt} = 21 embryos, 97 axons, $n^{col15a1b-/-}$ = 13 embryos, 54 axons, $n^{tnc-/-}$ = 13 embryos, 56 axons. (*E* and *F*) Statistical analyses were performed using Kruskal–Wallis and Dunn's multiple comparisons tests, median and range are represented. In all graphs, each point represents one motor axon. ns, not significant; **P* < 0.05, ***P* < 0.01, ****P* < 0.001, *****P* < 0.0001. All embryos are lateral views; anterior is left.

To assess the essential functions of TnC *versus* ColXV-B, we generated the double mutant line *col15a1b*$^{-/-}$; *tnc*$^{-/-}$ by crossing the two single mutant lines. Analysis of the axon phenotype revealed a reduction in axon length without impacting the total branching length (*SI Appendix*, Fig. S6 *A* and *B*). No significant developmental delay was observed in the double mutant embryos, that should be the most affected (*SI Appendix*, Fig. S6 *C* and *D*). We conclude that the disorganization of TnC in *col15a1b*$^{-/-}$ results in a detrimental gain-of-function. Next, to determine whether the neuro-muscular junction (NMJ) forms normally in the *tnc*$^{-/-}$ and *col15a1b*$^{-/-}$ embryos, we analyzed the synaptic areas in 27 hpf mutants and wild type at the horizontal myoseptum, a major synaptic site for initial motor axon synapses (24). Synaptic area (SyA) measurements that correspond to the overlap of presynaptic areas (znp-1 antibodies) and postsynaptic areas (α-bungarotoxin) labeling revealed that contrary to *tnc*$^{-/-}$ embryos, lack of *col15a1b* resulted in a higher synaptic area (*SI Appendix*, Fig. S5 *D* and *E*). This is not surprising as we previously showed that ColXV-B deposits coincide with axon varicosities where axons make synaptic contacts (14). Tnc and ColXV-B deposition in the motor path by SMPs both depend on MusK signaling (10, 14). In agreement with these data, our RNAseq analysis revealed that the onset of *musk* expression slightly precedes *col15a1b* expression, while *chrna1* expression starts along with *tnc* in premigratory SMPs (clusters 5 and 1) (*SI Appendix*, Fig. S5*F*), suggesting a role of ColXV-B in the formation or localization of the NMJ.

ColXV-B Deposits Adjust Motor Axon Microenvironment Stiffness Critical for Outgrowth. ColXV-B is a hybrid collagen/proteoglycan molecule as it carries glycosaminoglycan (GAG) chains, that are predominantly chondroitin sulfate (CS) chains in mammals (25) and in zebrafish as shown in *SI Appendix*, Fig. S7. The highly negatively charged GAG chains allow proteoglycans to sequester water that confers to tissues specific mechanical properties. There is growing evidence that axon elongation is influenced by tissue mechanics albeit differences in the response to the stiffness are observed depending on the type of neurons (26). To investigate the impact of microenvironment stiffness in motor axon navigation, we prepared polyacrylamide hydrogels with different degrees of stiffness ranging from 5 kPa to 40 kPa. Hydrogels were coated with laminin, a well-known potent attractive ECM cue, to allow the motor neuron neurites to grow. Isolated 24 hpf *mnx1:gfp* motor neurons were cultivated for 24 h and neurite growth was imaged (Fig. 6*A*) and measured as the total length of master segments per cell and the total branch length per cell using Fiji software (Fig. 6*B*). Quantification significantly shows that motor neurons develop more neurites when seeded onto soft hydrogels compared to stiff ones (5 kPa vs. 40 kPa; Fig. 6*B*) indicative of a possible mechanism of action for ColXV-B by providing growing motor axons with a permissive soft microenvironment. To test this assumption, we next examined whether in vivo ColXV-B deposits act on motor axon navigation by influencing the mechanical property in the vicinity of the motor axon path. We used atomic force microscopy (AFM) coupled to a fluorescent macroscope to measure the relative stiffness (elastic modulus) of frozen tissue sections, as previously reported (27–29). To accurately locate motor axons, we used 27 hpf *mnx1:gfp* and *col15a1*$^{-/-}$*;mnx1:gfp* embryos. The results show that the motor axon path is stiffer in absence of ColXV-B (mean$^{col15a1b-/-}$ = 447.5 kPa) relative to the wt (mean^{wt} = 151.92 kPa) (Fig. 6*C*). Noticeably, injection of *shh* mRNA in one cell stage embryos that was shown to increase deposition of ColXV-B in the motor path (14) leads to a significant decrease of the motor path stiffness (mean$^{shh\text{-injected}}$ = 106.67 kPa) compared to wt (Fig. 6*C*). Our findings add weight to the current belief that mechanosensing is critical for motor axon growth independently of chemical signals. In support to this, we have unraveled a mechanical role for ColXV-B in providing motor axons with a permissive soft ECM motor path.

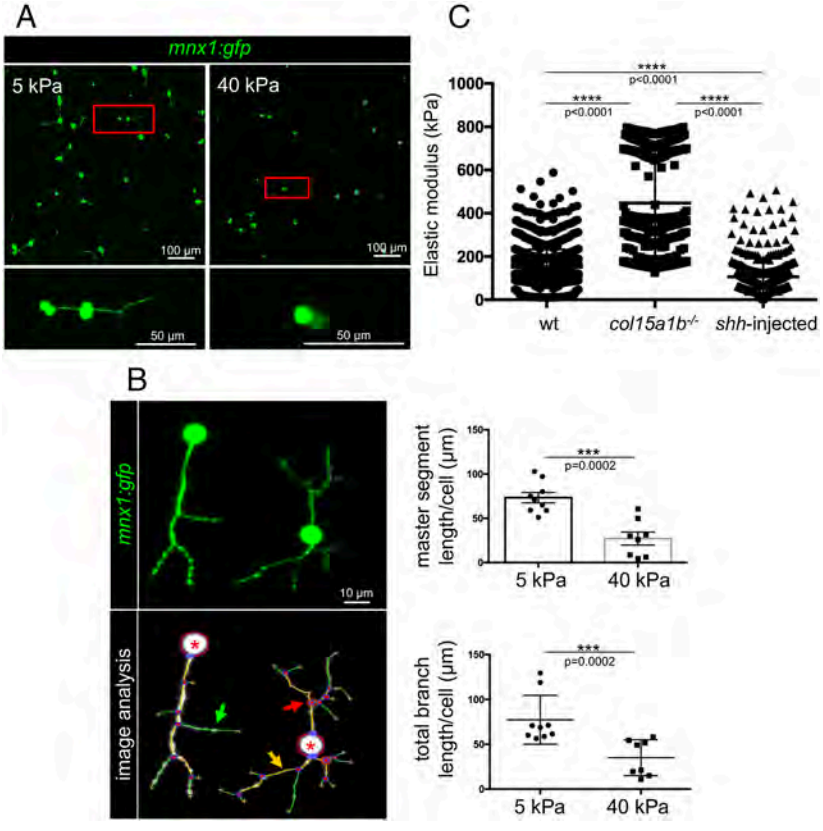

Fig. 6. ColXV-B locally creates a soft microenvironment that elicits motor axon growth. (*A*) Confocal images of 27 hpf *mnx1:gfp* motor neurons cultivated on 5 or 40 kPa polyacrylamide hydrogels for 24 h. Zoomed images of the boxed areas are shown. (*B*) *Left*, initial image sample (*Upper* panel) and after image analysis using the customized version of "Angiogenesis Analyzer", ImageJ software (*Bottom* panel). Asterisks, motor neuron cell bodies; arrows indicate master segments (orange); neurite branch (green); master junction (red). *Right*, quantification of the total master segment length and total branch length per cell, 24 h after motor neurons seeding (n = 418 cells for 40 kPa gels; n = 803 cells for 5 kPa gels). Triplicates of three independent experiments are represented. Statistical analysis was performed using a Student's *t*-test. Mean and SEM are presented. ***P < 0.001. (*C*) Elastic modulus in the motor axon path obtained from cryosections of 27 hpf wt, *col15a1b*$^{-/-}$ and *shh*-injected embryos in *mnx1:gfp* background. Statistical analysis was performed using Kruskal–Wallis and pairwise Wilcoxon multiple comparisons tests. *P < 0.05. n^{wt} = 1,342, n$^{col15a1b-/-}$ = 690, n$^{shh\text{-injected}}$ = 400. Data are mean ± SEM.

Discussion

Decades of research have shown that ECM contact–mediated cues locally influence axon navigation and pathfinding. Nevertheless, the identity of the ECM constituents along the motor path and the mechanism of their assembly that provide an extrinsic axon growth–promoting environment were not known. Here, we show that differentiating SMPs represent a major local source of ECM guidance cues, repellents, and/or attractants whose dual function is reflected by a dual topology tailored to influence motor axon shape and growth during development.

Classic in situ hybridizations previously showed that developing SMPs (a.k.a. adaxial cells) expressed ECM genes such as *col15a1b* whose expression is detected in 13 hpf embryos (30) while *tnc* and *col19a1* transcripts were respectively detected in 16 hpf (10) and 19hpf (13) embryos. Using scRNAseq, we characterized the repertoire of ECM genes expressed by differentiating SMPs and their temporal expression. A total of 36 core-matrisome genes are expressed by differentiating SMPs in both an overlapping and sequential pattern, providing ample evidence that SMPs are major local producers of the motor path ECM components. Importantly, our study assigns a specific gene signature to the principal morphological changes that SMPs undergo during their differentiation and hence sheds light on the understanding of the SMP lineage in zebrafish.

Our STRING analysis of SMP matrisomes reveals that most of the core-matrisome gene products interact to form a specialized BM containing both interlocked typical BM proteins and specific BM-associated proteins, namely TnC, ColXVIII, ColXIX, and ColXV-B. While BM are built with major components found in all BM (a.k.a. the BM toolkit), they can display more complex composition and distinct physical properties that serve tissue-specific functions (31). Interestingly, TnC, ColXVIII, ColXIX, and ColXV-B have all been reported to influence motor axon navigation in zebrafish during axon development (10, 12–14), although only TnC (10) and ColXV-B (14) proteins were reported to be physically present in the axonal microenvironment. Using double immunostaining and loss of function studies, we show that ColXV-B and TnC organize in a unique dual-topology that ideally serve axon navigation during development. By using bioprinted micropatterns that resemble motor axon path, we further validated these findings and demonstrate that the dual-topology of the ColXV-B and TnC immobilized cues is not only necessary but sufficient to control neurite navigation. Specialized BM have been described in several tissues including in different areas of the same cell, such as the myotendinous junction and the neuromuscular junction in myofibers (32). Together, our data spot the motor path as a specialized BM whose composition and topology are tailored to locally guide motor axon toward their muscle target.

Tnc and ColXV-B deposition in the motor path by SMPs both depend on MusK signaling (10, 14) and ColXV-B immunoreactivity coincides with synaptic contacts (14). Our scRNAseq data further revealed that *musk* and *col15a1b* are coexpressed in intermediate stages while *chrna1* (AChR) and *tnc* expression peaked in premigrating SMPs. We also identified *col15a1b* as the earliest BM-associated gene expressed in differentiated SMPs. Accordingly, we showed that lack of ColXV-B leads to impaired TnC organization in the motor path. Conversely, absence of TnC has no effect on ColXV-B organization. This is in line with previous findings suggesting that human Collagen XV acts as an ECM organizer in cell assays and in tissue (23, 33). As such, the absence of ColXV-B indirectly results in a significant increase in axon branching, a phenotype described in TnC morphants (10) and confirmed in our study using our *tnc* KO line. Likewise, when plated onto TnC substrate, neurites grew straight from chick spinal cord explants and displayed rare branches (34). However, the complete absence of TnC and its disorganization due to the lack of ColXV-B are not functionally equivalent, highlighting the subtle role of TnC in motor axon growth, contingent on its topology. The absence of both genes results in a predominant axonal length phenotype, while axon branching length remains unaffected. This suggests that TnC functions as a physical barrier. These findings underscore the importance of ECM topology in motor axon navigation beyond the mere expression of ECM cues.

Together, these data suggest that, in addition to its role in axon guidance, ColXV-B may orchestrate the organization of SMP-derived ECM proteins to make the ECM motor path fully functional.

There is compelling evidence that growing neurons respond not only to chemical but also to mechanical signals. Axons can sense and respond to the mechanical property of their close environment (35, 36). The mechanisms underlying durotaxis are not fully elucidated. It is however well recognized that neurons are able to sense variation in their microenvironment stiffness through receptors localized at the growth cone (26). Shortage of the mechanosensitive ion channel Piezo1 provoked axon pathfinding errors in *Xenopus* retinal ganglion cells (35). Yet, it is difficult to correlate local change in mechanical properties in vivo to slight but specific changes in ECM composition and organization. We show here that zebrafish motor axons are mechanosensitive and favorably extend neurites on soft substrate. Zebrafish ColXV-B carries chondroitin sulfate chains (*SI Appendix*, Fig. S7), as its human and mouse counterpart (25). Proteoglycans contribute to tissue viscoelasticity through their negatively charged sulfated glycosaminoglycans that are capable to bind and retain water in tissues (37). In vivo application of chondroitin sulfate chains to the *Xenopus* brain decreased its stiffness and subsequently affected the trajectory of RGC axons (35). Lack of Collagen XV in mice resulted in a significant increase of the cardiac ECM stiffness (23). Along this line, our data suggest that the presence of chondroitin sulfate chains imparts unique mechanical properties to ColXV-B, locally perceived as a permissive signal for motor axon growth.

In conclusion, we demonstrate the central role of myotomal ColXV-B in the elaboration of a specialized BM with unique topology and mechanical properties that are locally critical for motor axon shape and navigation, corroborating the assumption that *COL15A1* should be viewed as a candidate gene for neuromuscular disorders and peripheral neuropathies with unresolved genetic cause. Last but not least, our study not only provides fundamental insight into how ECM temporally and spatially orchestrates axonogenesis in vertebrates but will also help in the development of biomimetic ECM micropatterned scaffolds designed to promote peripheral nerve regeneration.

Materials and Methods

Fish Strain and Maintenance. Zebrafish (AB/TU) maintenance and embryo collection were performed at the zebrafish PRECI facility (Plateau de Recherche Expérimentale de Criblage In vivo, UMS CNRS 3444 Lyon Biosciences, Gerland) in compliance with French government guidelines. Embryos obtained from natural spawning were raised following standard conditions. Developmental stages are given in hours post-fertilization (hpf) at 28.5 °C according to morphological criteria (38).

Generation of the Mutant Lines. The *col15a1b* mutant strain carrying a nonsense mutation (*col15a1b*^{sa12573} allele) was obtained from the European Zebrafish Resource Center (Eggenstein-Leopoldshafen, Germany). Fish genotyping was performed as previously (14). *tnc*^{2stopex3} mutant (referred to as *tnc*$^{-/-}$) zebrafish line was generated using CRISPR/Cas9 mediated genome editing according to Gagnon et al. (39). A stop codon cassette was introduced leading to a premature termination codon in exon 3 (*SI Appendix*). Both mutant lines were outcrossed with Tg(*mnx1:gfp*) line to visualize motor neurons. The generation and

genotyping of the double mutant *col15a1b*$^{-/-}$;*tnc*$^{-/-}$;Tg(*mnx1:gfp*) is described in *SI Appendix*. All procedures have been approved by the local ethical committee and the Ministry of Higher Education and Research (APAFIS#27917-2020080513436447v7, APAFIS #37965-2022051900255627 v4).

Production and Characterization of Recombinant Proteins. Murine TnC (mrTnC) and ColXV-B NC1 domains (rNC10) were recombinantly produced in HEK-293 cells and purified as described in *SI Appendix*. The ColXV-B was produced in HEK_293 cells as previously described (3). Digestion with Chondroitinase ABC of recombinant ColXV-B followed by western blot analysis of the digested products and In Cell ELISA were used to analyze the presence of chondroitin sulfate on ColXV-B molecule as detailed in *SI Appendix*.

Production of Antibodies against ColXV-B (anti-NC1). The purified ColXV-B NC1 domains (rNC1) were used to immunize the guinea pig as described in *SI Appendix*, and the resulting anti-rNC1 antibodies were analyzed for their specificity with whole-mount immunofluorescence staining of 27 hpf embryos (*SI Appendix*, Fig. S2*B*).

Fluorescence-Activated Cell Sorting (FACS). To isolate slow muscle progenitors at 18 hpf, 75 pg of the *smyhc1:gfp* plasmid was injected into one-cell-stage AB/TU embryos (gift from Stone Elworthy, University of Sheffield, United Kingdom). For motor neurons isolation, we used 24 hpf *mnx1:gfp* zebrafish embryos to isolate motor neurons following the same protocol as for slow muscle cells. GFP^{+} cells were selected by FACS (FACSCANTO, ANIRA-cytometry, UMS 3444, SFR Biosciences Gerland, France) and immediately used for scRNAseq, micropatterns, or PAA hydrogels assays. Details are given in *SI Appendix*.

Single-Cell RNA Sequencing Analysis and Bioinformatics. ScRNAseq of GFP^{+} FACS-sorted cells was performed using 10× Genomics technology, and scRNAseq data were processed as described in *SI Appendix*. Raw reads for this project were deposited to SRA database under BioProject accession number PRJNA973246 (https://www.ncbi.nlm.nih.gov/bioproject/PRJNA973246) (40).

Single Molecule Inexpensive FISH (smiFISH). The design of the *col15a1b* and *tnc* smiFISH *probes* and the smiFISH procedure are described in *SI Appendix*. The list of the probes used for the experiments is provided in *SI Appendix*, Table S6.

Immunofluorescent Staining, Image Analysis, and Quantification. Whole-mount immunostainings of 27 hpf embryos were performed as previously described (14) and detailed in *SI Appendix*. After immunostaining, embryos were imaged at the level of the yolk sac extension (at the level of somites 10 to 12) covering 4 to 5 somites using an inverted confocal microscope (Zeiss LSM 780). Images are 3D projections using Imaris software or Image J *Z* projections of confocal *Z* stacks as indicated in the figure legends. Images were acquired with identical confocal settings and were equally posttreated with ImageJ software to value differences in signal intensity and image analysis and quantification were performed as detailed in *SI Appendix*. Briefly, to quantify motor neuron morphology, motor axons were selected in each of the five consecutive somites by making a new region of interest and by post-processing the images using Zen imaging software from Zeiss. Individual images were randomly renamed to work as blind. For branching length and branching points, we used filament tracer from Imaris software (Bitplane) as in ref. 41.

Mathematical Analysis of TnC Channel-Like Organization. An unsupervised clustering analysis was conducted to discriminate the TnC channel organization between wt and *col15a1b*$^{-/-}$ mutant embryos. First, each eight-bit image was truncated horizontally (*x* axis) around the channel center to focus on a common area of interest: the motor path. Following the truncation, the TnC distribution along the motor path of each image was estimated by vertically (along the *y* axis) summing nonzero pixels. The resulting distribution curves were smoothed by a Gaussian filter to remove spurious noise and normalized. A dissimilarity matrix was then built by evaluating the Hellinger distance, between each pair of curves. Finally, a graph partition was constructed from the dissimilarity matrix with the Leiden algorithm to cluster together similar eight-bit images. Mathematical background of each step is detailed in *SI Appendix*.

Double Micropatterning. The TnC/ColXV-B double micropatterned coverslips were prepared using the PRIMO system (Alveole Lab, France) mounted on an epifluorescence microscope (Nikon Eclipse Ti2). FACS-isolated motor neurons were seeded on micropatterns, and GFP fluorescence was acquired on inverted Zeiss LSM850 confocal (for details see *SI Appendix*).

Polyacrylamide Hydrogel Substrates and Neurite Tracing. PAA hydrogels of 5 and 40 kPa were prepared as previously described (42) and further detailed in *SI Appendix*. FACS-sorted motor neurons were seeded on PAA gels for 24 h at 28 °C and live-imaged on the Zeiss confocal microscope (LSM780). Neurite tracing and image analysis was performed using Fiji macro as detailed in *SI Appendix*.

Atomic Force Microscopy. Experiments were carried out using an atomic force microscope (Bioscope Catalyst-Bruker®) coupled with a fluorescent macroscope (MacroFluo, Leica). Elastic modulus of the motor axon microenvironment was measured on frozen sections. Elastic modulus quantification was performed with Nanoscope Analysis software (Bruker) (*SI Appendix*).

Statistical Analysis. Statistical analyses were carried out using GraphPad Prism. Depending on the experiments, the statistical methods to compare datasets were different and include the Shapiro–Wilk test, Student's *t*-test, Kruskal–Wallis test, pairwise Wilcoxon test, Kolmogorov–Smirnov test, Mann–Whitney test, and one-way ANOVA as indicated in the legend of the figures.

Data, Materials, and Software Availability. Raw data have been deposited in BioProject (PRJNA973246) (40). All other data are included in the manuscript and/or *SI Appendix*.

ACKNOWLEDGMENTS. We are grateful to Dr. Gertraud Orend (University of Strasbourg) for her helpful advice in handling Tenascin C and to Jonathan Enriquez, Mathilde Bouchet, Chloé Exbrayat-Héritier, and Alice Hugues (ENS de Lyon) for their invaluable assistance in smi-FISH experiments and image acquisition. We thank Guillaume Marcy (University of Lyon), Nathan Gil, and Camille Guillermin (ENS de Lyon) for their help with bioinformatics and Thomas Boudou (University Grenoble-Alpes) for his assistance in the fabrication of hydrogels. We acknowledge SFR Biosciences (Lyon, France) facilities (Laure Bernard, Robert Renard, and Sébastien Dussurgey) and Denis Ressnikoff (University Lyon 1) for his assistance in image analysis. This work was supported by the "Association Française de Myologie" (AFM #21064) to F.R. and by the EquipEx+ Spatial-Cell-ID under the "Investissements d'avenir" program (ANR-21-ESRE-00016). L.N.-B. is a recipient of a "Ministère de l'Enseignement Supérieur et de la Recherche" PhD fellowship. I.S. is a recipient of a FRM postdoc fellowship (SPF201909009228).

Author affiliations: [a]Institut de Génomique Fonctionnelle de Lyon, Ecole Normale Supérieure de Lyon, UMR5242 CNRS, Université Claude Bernard-Lyon1, National Research Institute for Agriculture, Food and the Environment (INRAe) Unit under Contract (USC) 1370, Lyon 69007, France; [b]LIPphy: Interdisciplinary Laboratory of Physics, Université Grenoble Alpes, CNRS, Grenoble F-38000, France; [c]Gly-CRRET: Glycobiology, Cell Growth and Tissue Repair Research Unit, Laboratoire Gly-CRRET Faculté des Sciences et Technologie, Université Paris Est-Créteil-Val de Marne, Créteil Cedex 94010, France; and [d]Institute for Experimental Dental Research and Oral Musculoskeletal Biology, Center for Biochemistry, Medical Faculty, University of Cologne, Cologne 50931, Germany

1. B. J. Dickson, Molecular mechanisms of axon guidance. *Science* **298**, 1959–1964 (2002).
2. C. E. Beattie, Control of motor axon guidance in the zebrafish embryo. *Brain Res. Bull.* **53**, 489–500 (2000).
3. E. Melançon, D. W. C. Liu, M. Westerfield, J. S. Eisen, Pathfinding by identified zebrafish motoneurons in the absence of muscle pioneers. *J. Neurosci.* **17**, 7796–7804 (1997).
4. J. Zhang, M. Granato, The zebrafish *unplugged* gene controls motor axon pathway selection. *Development* **127**, 2099–2111 (2000).
5. D. F. Daggett, C. R. Domingo, P. D. Currie, S. L. Amacher, Control of morphogenetic cell movements in the early zebrafish myotome. *Dev. Biol.* **309**, 169–179 (2007).
6. H. L. Stickney, M. J. F. Barresi, S. H. Devoto, Somite development in zebrafish. *Dev. Dyn.* **219**, 287–303 (2000).
7. S. Ricard-Blum, F. Ruggiero, The collagen superfamily: From the extracellular matrix to the cell membrane. *Pathol. Biol.* **53**, 430–442 (2005).
8. R. R. Bernhardt, M. Schachner, Chondroitin sulfates affect the formation of the segmental motor nerves in zebrafish embryos. *Dev. Biol.* **221**, 206–219 (2000).
9. J. Zhang, J. L. Lefebvre, S. Zhao, M. Granato, Zebrafish unplugged reveals a role for muscle-specific kinase homologs in axonal pathway choice. *Nat. Neurosci.* **7**, 1303–1309 (2004).

10. J. Schweitzer *et al.*, Tenascin-C is involved in motor axon outgrowth in the trunk of developing zebrafish. *Dev. Dyn.* **234**, 550–566 (2005).
11. S. Bretaud, P. Nauroy, M. Malbouyres, F. Ruggiero, Fishing for collagen function: About development, regeneration and disease. *Seminars Cell Dev. Biol.* **89**, 100–108 (2019).
12. V. A. Schneider, M. Granato, The Myotomal diwanka (lh3) glycosyltransferase and type XVIII collagen are critical for motor growth cone migration. *Neuron* **50**, 683–695 (2006).
13. J. D. Hilario, C. Wang, C. E. Beattie, Collagen XIXa1 is crucial for motor axon navigation at intermediate targets. *Development* **137**, 4261–4269 (2010).
14. E. Guillon, S. Bretaud, F. Ruggiero, Slow muscle precursors lay down a collagen XV matrix fingerprint to guide motor axon navigation. *J. Neurosci.* **36**, 2663–2676 (2016).
15. F. Meyer, B. Moussian, Drosophila multiplexin (Dmp) modulates motor axon pathfinding accuracy: Dmp modulates motor axon pathfinding. *Dev. Growth Different.* **51**, 483–498 (2009).
16. B. D. Ackley *et al.*, The Nc1/Endostatin domain of Caenorhabditis elegans type Xviii collagen affects cell migration and axon guidance. *J. Cell Biol.* **152**, 1219–1232 (2001).
17. S. Baxendale *et al.*, The B-cell maturation factor Blimp-1 specifies vertebrate slow-twitch muscle fiber identity in response to Hedgehog signaling. *Nat. Genet* **36**, 88–93 (2004).
18. B. Thisse *et al.*, "Spatial and temporal expression of the zebrafish genome by large-scale in situ hybridization screening" in *Methods in Cell Biology* (Elsevier, 2004), pp. 505–519.
19. B. Thisse, C. Thisse, Functions and regulations of fibroblast growth factor signaling during embryonic development. *Dev. Biol.* **287**, 390–402 (2005).
20. C. Thisse, B. Thisse, High-resolution in situ hybridization to whole-mount zebrafish embryos. *Nat. Protoc* **3**, 59–69 (2008).
21. P. Nauroy, S. Hughes, A. Naba, F. Ruggiero, The in-silico zebrafish matrisome: A new tool to study extracellular matrix gene and protein functions. *Matrix Biol.* **65**, 5–13 (2018).
22. P. Strale *et al.*, Multiprotein printing by light-induced molecular adsorption. *Adv. Materials* **28**, 2024–2029 (2016).
23. K. Rasi *et al.*, Collagen XV is necessary for modeling of the extracellular matrix and its deficiency predisposes to cardiomyopathy. *Circ Res.* **107**, 1241–1252 (2010).
24. J. A. Panzer *et al.*, Neuromuscular synaptogenesis in wild-type and mutant zebrafish. *Dev. Biol.* **285**, 340–357 (2005).
25. S. Bretaud, E. Guillon, S.-M. Karppinen, T. Pihlajaniemi, F. Ruggiero, Collagen XV, a multifaceted multiplexin present across tissues and species. *Matrix Biol. Plus* **6**, 100023 (2020).
26. A. I. M. Athamneh, D. M. Suter, Quantifying mechanical force in axonal growth and guidance. *Front. Cell. Neurosci.* **9**, 359 (2015).
27. N. R. Chevalier, E. Gazguez, S. Dufour, V. Fleury, Measuring the micromechanical properties of embryonic tissues. *Methods* **94**, 120–128 (2016).
28. C. Roduit *et al.*, Stiffness tomography exploration of living and fixed macrophages: Macrophages mechanical properties. *J. Mol. Recognit.* **25**, 241–246 (2012).
29. P. Nauroy *et al.*, Gene profile of zebrafish fin regeneration offers clues to kinetics, organization and biomechanics of basement membrane. *Matrix Biol.* **75**, 82–101 (2019).
30. S. Bretaud, A. Pagnon-Minot, E. Guillon, F. Ruggiero, D. Le Guellec, Characterization of spatial and temporal expression pattern of Col15a1b during zebrafish development. *Gene Exp. Patt.* **11**, 129–134 (2011).
31. D. R. Sherwood, Basement membrane remodeling guides cell migration and cell morphogenesis during development. *Curr. Opin. Cell Biol.* **72**, 19–27 (2021).
32. J. R. Sanes, The basement membrane/basal lamina of skeletal muscle. *J. Biol. Chem.* **278**, 12601–12604 (2003).
33. M. Hurskainen, F. Ruggiero, P. Hägg, T. Pihlajaniemi, P. Huhtala, Recombinant human collagen XV regulates cell adhesion and migration. *J. Biol. Chem.* **285**, 5258–5265 (2010).
34. B. Wehrle, M. Chiquet, Tenascin is accumulated along developing peripheral nerves and allows neurite outgrowth in vitro. *Development* **110**, 401–415 (1990).
35. D. E. Koser *et al.*, Mechanosensing is critical for axon growth in the developing brain. *Nat. Neurosci.* **19**, 1592–1598 (2016).
36. G. F. Martínez *et al.*, Extracellular matrix stiffness negatively affects axon elongation, growth cone area and F-actin levels in a collagen type I 3D culture. *J. Tissue Eng. Regen. Med.* **16**, 151–162 (2022).
37. B. J. Murienne, J. L. Jefferys, H. A. Quigley, T. D. Nguyen, The effects of glycosaminoglycan degradation on the mechanical behavior of the posterior porcine sclera. *Acta Biomaterialia* **12**, 195–206 (2015).
38. C. B. Kimmel, W. W. Ballard, S. R. Kimmel, B. Ullmann, T. F. Schilling, Stages of embryonic development of the zebrafish. *Dev. Dyn.* **203**, 253–310 (1995).
39. J. A. Gagnon *et al.*, Efficient mutagenesis by Cas9 protein-mediated oligonucleotide insertion and large-scale assessment of single-guide RNAs. *PLoS One* **9**, e98186 (2014).
40. L. Nemoz-Billet, S. Bretaud, F. Ruggiero, Data from "Expression profiles of zebrafish differentiating slow muscle precursors". BioProject. https://www.ncbi.nlm.nih.gov/bioproject/PRJNA973246. Deposited 17 May 2023.
41. L. Nemoz-Billet, J. Brocard, F. Ruggiero, S. Bretaud, Quantitative image analysis of axonal morphology in in vivo model. *MPs* **6**, 116 (2023).
42. J. R. Tse, A. J. Engler, Preparation of hydrogel substrates with tunable mechanical properties. *Curr. Protocols Cell Biol.* **47**, 1–16 (2010).